DEROA: A Differential Evolution Rolling Optimization Approach for Multi-UAV Trajectory Planning based on Spatial Grid Probability Map

Jiayuan Cheng¹, Xiaochong Tong¹*, Hao Guo¹, Yuekun Sun¹, Jiayi Tang¹, Chang Yuan¹, Liang Song¹

Keywords: Multi-UAV Systems, Cooperative Perception, Probabilistic Quantification Grid Map, Differential Evolution, Rolling Optimization, Path Planning.

Abstract

With large-scale UAV swarms used in wide-area inspection, multi-UAV cooperative perception faces core challenges like uneven target distribution and inefficient paths, causing blind planning with risks of redundant detection or misses. To address traditional method limitations in real-time target existence probability quantification and dynamic path optimization, this paper proposes the Differential Evolution Rolling Optimization path planning method (DEROA) based on a spatial grid probability map. Using a constructed target grid probability map, DEROA dynamically updates the paths as the probabilities of the grid evolve, in order to maximize the probability of general perception expectation of the multi-UAV system. The main innovations are as follows: (1) A probabilistic quantification grid map with multisource information fusion for inspection targets integrates historical trajectories, geographical obstacles, and real-time perception data. Dynamically updates grid target existence probabilities via Bayesian inference to direct UAVs to high-probability areas, addressing the deficiency of traditional modeling in representing dynamic target distributions. (2) The differential evolution-based rolling optimization cooperative algorithm combines DE's global search capability with rolling horizon optimization's real-time adjustment, achieving gridded dynamic path planning through distributed model redictive control. Experiments show that DEROA improves high-probability area coverage by 65.7%-106.6% and 1.0%-10.9% compared to traditional algorithms, with non-faulty UAV task coverage maintaining 0.44-0.97 under failure mechanisms, demonstrating strong robustness. (3) A dynamic reward function incorporating collision avoidance, communication constraints, and energy consumption, coupled with a path inflection point simplification algorithm reducing flight turns by 40%-60%, enables DEROA to achieve a maximum target discovery probability of 0.62 (3.3%-37.8% improvement), significantly enhancing perception efficacy in large-area scenarios.

1. Introduction

The deep integration of Unmanned Aerial Vehicle (UAV) technology and Artificial Intelligence (AI) (Hashesh et al., 2022)has demonstrated the critical value of multi-UAV systems in scenarios such as military reconnaissance (Alexan et al., 2024), situational awareness (Baek and Lim, 2018), emergency response (Boccardo et al., 2015), and environmental monitoring (Asadzadeh et al., 2022). However, single UAVs are constrained by limitations in endurance, sensing range, and decision-making capabilities. When confronted with complex tasks, they are prone to inefficiencies and difficulties in localized decisionmaking. These shortcomings also hinder the development of multi-UAV systems. Consequently, multi-UAV cooperative planning has emerged as a key research focus (Xu et al., 2020). By enabling collaborative cooperation among multiple UAVs, it effectively enhances mission execution efficiency and mitigates the operational constraints inherent to single-UAV operations (Wu et al., 2022).

The efficient realization of multi-UAV cooperative perception relies on the accuracy of environmental models and the decision-making capabilities of individual UAVs. The spatial structure and target probability quantification within environmental models determine the rationality of task allocation (Peng et al., 2022). Environmental modeling often struggles to adapt to target motion and dynamic scenario changes, while single-agent algorithms are susceptible to local optima. This can lead to multi-UAV path conflicts, task redundancy, and ultimately constrain swarm effectiveness (Shahbazi et al., 2015).

In environmental modeling, the 2D grid mapping method discretizes the environment using regular grids to construct situational awareness information (Hügler et al., 2020). The grid-based approach fully leverages the computational advantages of grid systems for planning flight trajectories while incorporating UAV kinematic constraints (Xiao et al., 2021). The grid-based probability map method further refines this discretization, assigning each cell a target existence probability that enables precise quantification of high-value regions. This structured representation directly guides UAVs to prioritize areas with elevated detection potential.

Single-UAV path planning necessitates a balance between environmental adaptability and optimization efficiency. Mainstream algorithms fall into two categories: mathematical model-based approaches and swarm intelligence algorithms. While mathematical model-based algorithms can theoretically achieve optimal solutions (Rachman and Razali, 2011), their computational complexity increases exponentially with problem scale. Swarm intelligence algorithms (Zhou et al., 2020), such as Differential Evolution (DE) (Yu et al., 2020), characterized by few parameters and good robustness, offer significant advantages in multi-UAV cooperation. Multi-UAV collaborative decision-making requires solving the coupled challenge of "task allocation-trajectory planning-dynamic adaptation" (Li et al., 2022). Traditional decoupled strategies, applications of intelligent algorithms, and distributed frameworks exhibit deficiencies, with existing research showing gaps in constraint satisfaction, robustness, and adaptability (Sun et al., 2024).

¹ Institute of Geospatial Information, Information Engineering University, Zhengzhou, Henan 450001, China * Corresponding author, Email: txchr@zxiat.com, txchr@aliyun.com

To address these challenges, this study presents two core contributions:

- A multi-layer information fusion probabilistic quantification map model: The model integrates historical trajectories, geographical obstacles, and real-time data. This model dynamically updates grid target probabilities using Bayesian inference, directing UAVs to prioritize coverage of high-value areas and resolving the dynamic distribution representation deficiencies inherent in traditional modeling approaches (Elamin and El-Rabbany, 2022).
- 2. A Differential Evolution-based Rolling Optimization Cooperative Algorithm (DEROA): This approach combines the global search capability of the DE algorithm with the real-time adjustment strength of rolling optimization (Yu et al., 2017). By incorporating adaptive mechanisms and path simplification strategies, it provides an efficient planning solution for multi-UAV systems operating in complex scenarios.

The rest of this paper is organized as follows: Section 2 models multi-UAV cooperative tasks. Section 3 proposes the DEROA algorithm. Section 4 evaluates via experiments. Section 5 concludes and outlines future work.

2. Analysis and Modeling of Grid-Based Multi-UAV Cooperative Perception Planning Tasks

2.1 Problem Description

In large-area inspection missions, there exist M targets to be perceived $(Tar = \{T_1, T_2, \ldots, T_M\})$ within the region. N UAVs $(U = \{U_1, U_2, \ldots, U_N\})$ are deployed to perform cooperative detection. UAVs dynamically adjust their paths under limited spatio-temporal resources. Based on a gridded probability map and information sharing via ad-hoc networks, they form a "detection-feedback-planning" closed loop aimed at maximizing detection probability, minimizing energy consumption, and prioritizing coverage of high-probability areas.

2.2 Modeling of Cooperative Perception Elements

2.2.1 Environmental Modeling: The target area is discretized into a two-dimensional grid matrix using the grid method. Each grid cell has coordinates (i,j) and attributes including its location \log_i and target existence probability η_i (where $\eta_i=1$ indicates target presence). This gridded probability map, updated dynamically via Bayesian inference, fuses multi-source data (e.g., historical trajectories, terrain obstacles) to form a robust foundation for path planning. Grid size is determined based on target dimensions and sensor resolution. Paths between adjacent grids are formed by connecting their center points. By fusing prior data such as historical trajectories and terrain obstacles using Bayesian inference, the target probability per grid is dynamically updated, generating a probabilistic quantification map to guide path planning.

2.2.2 UAV Modeling: The state of a UAV is defined by its two-dimensional coordinates (x(t),y(t)) and yaw angle $\varphi(t)$. State transitions satisfy kinematic equations: position updates are based on velocity and yaw angle, while changes in the yaw angle are constrained by dynamics within the range $[-\pi/4,\pi/4]$. The flight direction is discretized into eight directions to construct a path decision tree.

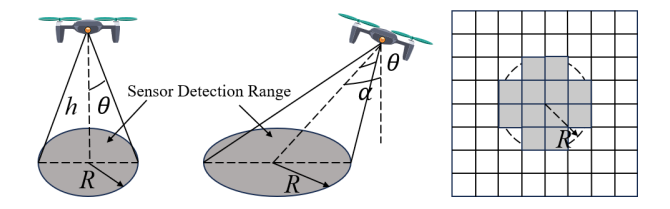


Figure 1. Schematic diagram of UAV sensor detection range mapping.

- **2.2.3 Sensor Modeling:** The sensor's downward-looking detection range is a circular area with radius $R = h \cdot \tan \theta$ (where h is altitude and θ is the field-of-view angle). The gimbal tilt angle α ranges within $[-\alpha_{\max}, \alpha_{\max}]$. The detection area becomes elliptical, with the semi-major axis radius extended to $R(\alpha) = h \cdot \tan(\theta + \alpha)$. As shown in Figure 1, the sensor detection range changes with the variation of relevant parameters.
- **2.2.4 Communication Modeling:** In multi-UAV cooperative missions, UAVs must maintain communication within an effective range. Let the maximum communication distance be d_c . Effective mission execution requires the distance d between any two UAVs to satisfy $d < d_c$.
- **2.2.5** Target Probability Map Modeling: For multi-UAV cooperative large-area inspection, target modeling requires constructing a probabilistic quantification map that integrates target attributes and environmental features. Taking vehicle targets as an example, the specific process is as follows:

Structured Fusion of Multi-Source Factors: After discretizing the target area into grids, multi-dimensional environmental data such as road distribution, terrain slope, and vegetation coverage are extracted. Road elements are assigned initial probabilities based on their presence. Terrain flatness is converted into probability values via normalized slope. Shelter and vegetation coverage are directly linked to regional survivability, enabling probabilistic representation of multi-source data.

Gaussian Buffer Expansion Mechanism: Gaussian Buffer Expansion Mechanism:Centered on road grids, buffer probabilities are generated using Eq. (1) to simulate the diffusion trend of targets along the road network. This overcomes the limitation of traditional grid methods in representing linear target distributions, making the probability map better conform to actual target migration patterns. The grid-based probability map employs this Gaussian buffer mechanism to simulate target diffusion, ensuring adaptability to linear distributions. Here, Ω_r denotes the set of all road grids, and σ controls the buffer extent.

$$p_{rb} = \sum_{(m,n)\in\Omega_r} \frac{1}{2\pi\sigma^2} \exp\left(-\frac{(i-m)^2 + (j-n)^2}{2\sigma^2}\right)$$
 (1)

where

 Ω_r = set of all road grids σ = buffer extent control parameter p_{rb} = buffer probability at grid (i,j)

Multi-Factor Linear Weighted Model: A linear weighted model integrates the factors to generate the target existence probability:

$$p_t = \omega_r \cdot p_{rb} + \omega_s \cdot p_s + \omega_c \cdot p_c + \omega_v \cdot p_v \tag{2}$$

where

 p_t = target existence probability at grid (i, j) $\omega_r, \omega_s, \omega_c, \omega_v$ =weights for different features p_s, p_c, p_v = probabilities for different factors

The weight coefficients satisfy $\omega_r + \omega_s + \omega_c + \omega_v = 1$. For instance, in constructing a road-target probability map, typical weights are: road feature weight $\omega_r = 0.7$, terrain flatness weight $\omega_s = 0.1$, shelter coverage weight $\omega_c = 0.1$, and vegetation coverage weight $\omega_v = 0.1$. This model, utilizing Gaussian buffering and linear weighting, generates a probability map that guides UAVs to prioritize detecting high-probability areas.

3. Grid-Based Path Planning Method for Multi-UAV Cooperative Perception Tasks

Addressing the bottlenecks of dynamic environment adaptation and path optimization efficiency in multi-UAV cooperative perception modeling, this chapter proposes DEROA. This algorithm integrates the This algorithm integrates the global search capability of Differential Evolution DE with the real-time adjustment strength of Rolling Horizon Optimization (RHO). Utilizing Distributed Model Predictive Control (DMPC), it constructs a reward function to achieve dynamic path planning for multiple UAVs.

3.1 Path Planning Method Based on DE Algorithm

The DE algorithm is well-suited for multi-UAV path planning due to its strong global search capability, low computational cost, and flexible parameter tuning. Its core process comprises four stages:

- 1. **Initialization:** Each UAV determines its initial position, direction, and population size, planning paths for the next L steps (individual dimension = L). Three turning strategies (0,-1,1) are generated via a random function as initial solutions. Parameter ranges are set according to flight constraints to cover the feasible search space.
- Selection: Three distinct individuals (turning strategy samples) are randomly selected from the population. An indexing mechanism prevents duplicate selection, ensuring sample diversity and providing foundational input for crossover.
- 3. Crossover: The original individual undergoes gene recombination with the three selected individuals based on a preset probability, generating an intermediate candidate solution. Random parameters determine whether new features (e.g., adjusting the turning strategy at specific steps) are retained, balancing global search capability with diversity in local path inflection points.
- 4. Mutation: Based on the difference information between the intermediate candidate solution and the three selected individuals, a mutant individual is generated via linear combination. A mutation factor controls the weight of the difference vector, regulating the magnitude of heading angle changes. This explores potential optimal solutions while preserving population diversity, generating candidate paths that balance path smoothness and global exploration capability.

3.2 Multi-UAV Cooperative Search Decision Strategy Based on DMPC

DMPC employs a decentralized architecture. Each UAV independently maintains a local prediction model based on kinematic equations, considering sensor and communication constraints. Through ad-hoc networking, UAVs share states and trajectories to form a cooperative group. Paths are optimized over a finite horizon in a rolling fashion within each control cycle to reduce computational complexity.

Building upon this, multi-UAV cooperative search forms a dynamic closed loop through state prediction, path optimization, and execution feedback: Trajectory decision trees are generated based on motion equations; paths are optimized using a multicriteria utility function; the map is updated during execution; the model is reconstructed using real-time data; and coordination is achieved via communication interaction.

3.3 Environmental Information Model

The environmental information model constructs a dynamic target probability update mechanism based on Bayesian inference. The target area is divided into discrete grids initialized with prior probabilities using multi-source environmental data. Real-time detection data is then fused to update the posterior probability, characterizing the target distribution.

First, define $P' = P(D^k_{i,j} \mid H^k_{i,j}) \cdot P(H^{k-1}_{i,j})$, which represents the joint probability of observing data $D^k_{i,j}$ under the hypothesis that the target exists in grid (i,j). The Bayesian update process is thus reformulated as:

$$P(H_{i,j}^k) = \frac{P'}{P' + P(D_{i,j}^k \mid \overline{H}_{i,j}^k) \cdot (1 - P(H_{i,j}^{k-1}))}$$
(3)

where

 $\begin{array}{l} P(H^k_{i,j}) = \text{posterior probability of target existence} \\ P(H^{k-1}_{i,j}) = \text{prior probability} \\ P(D^k_{i,j} \mid \overline{H}^k_{i,j}) = \text{probability (target absent)} \end{array}$

The Bayesian inference-based update mechanism continuously refines grid probabilities, ensuring the map remains responsive to real-time detection data. This dynamic grid representation is central to DEROA's ability to adapt to changing target distributions. This formula iteratively refreshes the probability map: the prior probability reflects historical knowledge; the observation probability reflects detection reliability; the posterior probability integrates both to form an environmental estimate.

Based on UAV detection feedback, the model updates the probability map to guide path planning towards high-probability areas.

3.4 Dynamic Reward Function

After generating candidate UAV paths via DE, evaluating path quality is critical. A dynamic reward function balances detection efficiency and constraints, with hard/weighted terms:

1. Collision Avoidance (Hard Constraint): This is a binary function for flight safety. Paths are infeasible if the Euclidean distance $E_{ij}(t)$ between two UAVs is less than the safety threshold d_1 . Only when the condition for feasible paths (i.e., $E_{ij}(t) \geq d_1$) is met, subsequent weighted optimization terms are calculated.

- 2. Communication Constraint (Weighted): It quantifies communication link effectiveness. The value is 1 if the Euclidean distance $E_{ij}(t)$ between two UAVs is less than or equal to the communication threshold d_2 (representing the information-sharing range), otherwise 0.
- Energy Consumption (Weighted): The number of UAV turns is used as the energy consumption metric. The formula is:

$$S_3^t(t) = 1 - \frac{\operatorname{turn}_{(t)}}{\operatorname{step}} \tag{4}$$

where

 $turn_{(t)} = UAV turns at t$ step = planning steps

4. **High-Probability Coverage (Weighted):** It integrates coverage assessment with high-probability area detection. The formula is:

$$S_4^t(t) = \frac{HC(t) + \Delta C(t)}{HC + C} \tag{5}$$

where

HC(t) = high-probability grids detected at t $\Delta C(t)$ = grid changes at t HC = initial high-probability grids C = initial unsearched grids

State-Dependent Weight Adjustment: UAVs operate in high-probability ($p_t > 0.6$) or low-probability ($p_t < 0.6$) areas. Weights adapt via:

$$S_{\text{in}}^{t}(t) = S_{1}^{t} \cdot \left(\beta_{2} S_{2}^{t} + \beta_{3} S_{3}^{t} + \beta_{4} S_{4}^{t}\right) \tag{6}$$

$$S_{\text{out}}^t(t) = S_1^t \cdot \left(\beta_2 S_2^t + \beta_3' S_3^t + \beta_4' S_4^t\right) \tag{7}$$

where

 $\beta_2, \beta_3, \beta_4$ = base weights β_3, β_4' = adjusted weights $0 < \beta_3' < \beta_3, \beta_4 < \beta_4' < 1$

High-Probability ($p_t > 0.6$): $\beta_2 = 0.2$, $\beta_3 = 0.3$, $\beta_4 = 0.5$ (Balances communication and energy consumption for sustained high - value coverage)

Low-Probability ($p_t < 0.6$): $\beta_2 = 0.2$, $\beta_3 = 0.1$, $\beta_4 = 0.7$ (Reduces energy-related weight, increases detection-related weight to guide UAVs to high-probability areas)

4. Experiments and Analysis

4.1 Experimental Design

- **4.1.1 Experimental Objectives:** To evaluate the practical effectiveness of the proposed DEROA algorithm in UAV path planning, the following three sets of experiments were designed:
 - 1. **Feasibility Experiment:** Conducted with 2, 5, and 10 UAVs, respectively, with randomly set faulty UAVs.
 - Robustness Experiment: Compared DEROA against mainstream PSO and greedy strategies under complex environments and varying mission scales.

- 3. **Planning Quality Experiment:** Based on the robustness experiment, statistically analyzed DEROA's average runtime and maximum target discovery probability to quantitatively assess its time complexity and planning accuracy.
- 4.1.2 Experimental Data and Environment: An area in Zhengzhou was selected as the inspection region, utilizing the probabilistic quantification map shown in Figure 2. This map discretizes the inspection area into a grid matrix of 118 km × 121 km, with each grid cell sized 1 km \times 1 km. The gridded probability map discretizes the inspection area into 1 km×1 km cells, with color depth reflecting target probability. This visualization highlights the grid structure critical for UAV path planning. The color depth of each grid cell maps to the target existence probability, where darker shades represent highprobability regions (0.6-1.0). Each grid is assigned a probability value between 0 and 1, characterizing the likelihood of target presence. These probability values were generated by fusing core factors such as road distribution. Specifically, the regional road network was extracted, and Gaussian buffering analysis with a buffer radius set to 5 km was applied to simulate the diffusion trend of targets along roads, resulting in the initial probability distribution. The UAVs used in the experiments were

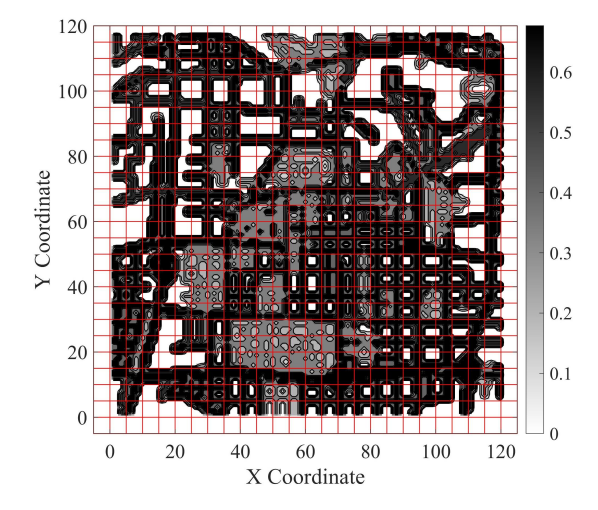


Figure 2. Vehicle target probability map of a specific area.

a common model, with parameters assumed based on publicly available data as follows: cruise speed of 80 km/h; maximum endurance per mission of 5 hours; sensor detection radius of 5 km (covering 5 to 10 grid cells on the map, corresponding to an actual coverage area of 100-200 km²); and communication range sufficient for multi-UAV cooperation within the region. All UAVs possessed identical payload capacity, endurance, and flight speed. Their kinematic model was simplified based on rigid-body dynamics, assuming straight-line flight at constant speed with a yaw angle variation range of $\pm 45^{\circ}$ and a minimum turning radius of 500 m.

The experimental hardware environment utilized an 11th Gen Intel(R) Core(TM) i5-1135G7 @ 2.40GHz processor, 16GB RAM, and Windows 10 x64 operating system. The algorithm was implemented in C++11 and compiled using Visual Studio 2022.

4.1.3 Experimental Evaluation Metrics:

 Grid Coverage Rate: The Grid Coverage Rate serves as the core metric for evaluating an algorithm's ability to cover high-probability target areas. Its calculation formula

$$C = \frac{N_c}{N_t} \tag{8}$$

where N_c = number of covered grid cells N_t = total grid cells

Maximum Target Discovery Probability: The Maximum Target Discovery Probability is a key metric for assessing detection effectiveness. Its calculation formula is:

$$P_{\text{max}} = 1 - \prod_{i=1}^{n} (1 - m_i) \tag{9}$$

where n = number of planning steps $m_i =$ target discovery probability

This formula calculates the probability of detecting the target at least once throughout the planned path by multiplying the complements of the non-detection probabilities at each grid cell.

4.2 Experimental Procedure

The experimental procedure comprises three key stages to comprehensively evaluate the DEROA algorithm, as detailed below:

- Feasibility Experiment Steps: For UAV counts of 2, 5, and 10 respectively, DEROA was employed for path planning. The generated paths were examined to ensure reasonable avoidance of known obstacles, verifying the solution's feasibility in basic scenarios.
- Robustness Experiment Steps: Path planning was performed using DEROA, PSO, and Greedy Strategy(GS) under varying environmental complexities. Each algorithm was independently executed 25 times under identical environmental settings, followed by comparative analysis of Grid Coverage Rate parameters.
- Planning Quality Experiment Steps: Path planning was conducted on prior probability maps incorporating road and shelter features under different reconnaissance time scales. The average runtime and Maximum Target Discovery Probability for DEROA, PSO, and GS were statistically recorded.

4.3 Experimental Results and Analysis

4.3.1 Feasibility Experiment Results and Analysis: Feasibility experiments employed 2, 5, and 10 UAVs, including randomly introduced faulty UAVs, during a 50-minute reconnaissance mission to validate DEROA's capability to generate collision-free paths and handle anomalies. As illustrated in Figures 3, 4, 5, UAVs across all counts successfully traversed high-probability regions from their starting points according to the planned paths. Faulty UAVs were correctly marked as "Faulty" without disrupting normal task execution.

The key metric, coverage rate, exhibited a trend where with 2 UAVs, the coverage rate was 0.44, primarily covering central high-probability regions (probability > 0.6); with 5 UAVs, coverage improved to 0.90, extending to peripheral regions (probability 0.3-0.5); and with 10 UAVs, coverage reached 0.97,

achieving uniform coverage across the entire region, including low-value areas (probability 0.1-0.2). This demonstrates that DEROA's collaboration mechanism effectively utilizes multi-UAV resources, with coverage showing near-exponential improvement as the UAV count increases.

Figure 3, 4, 5 depict the planned paths of UAVs focusing on high-probability regions within the area. The figures illustrate task execution for 2, 5, and 10 UAVs, respectively. Individual UAV routes are distinguished by different colors, clearly showing their traversal paths from starting points through high-probability zones based on the grid map. The visualization intuitively presents the detection coverage pattern of individual UAVs over high-probability areas and the collaborative detection coverage effectiveness of multiple UAVs operating simultaneously. Operational UAV paths exhibited 40%-60% fewer turns compared to traditional spiral scanning patterns. For example, UAV 1 in the 10-UAV case (Figure 5) flew straight from (91,22) to (91,47), demonstrating no redundant inflection points and confirming the efficacy of the path simplification algorithm.

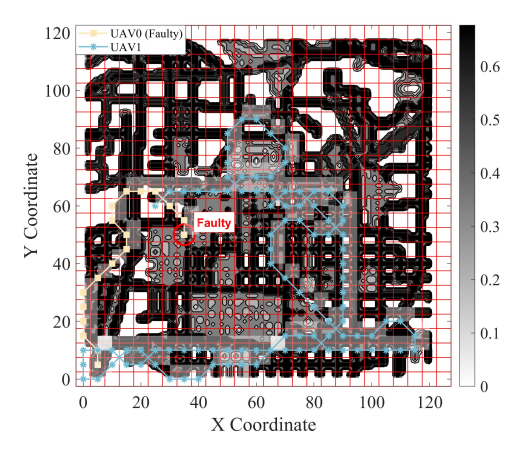


Figure 3. 2 UAVs: High-Probability region paths.

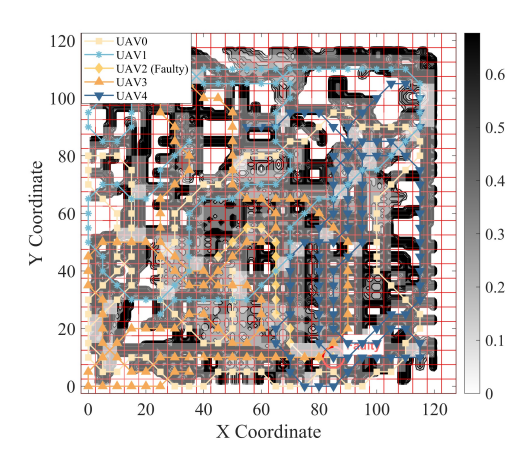


Figure 4. 5 UAVs: High-Probability region paths.

4.3.2 Robustness Experiment Results and Analysis: Table 1 lists the overall average coverage and variance for the three algorithms. Results exhibiting significant differences compared to the other two algorithms are marked in bold. The confidence level for hypothesis testing was set at $\alpha=0.05$, indicating the decision risk level (Liang et al., 2023).

In the low reconnaissance time scenarios (30-50 min), the coverage rate of DEROA is 0.70-0.87. Compared to GS, it in-

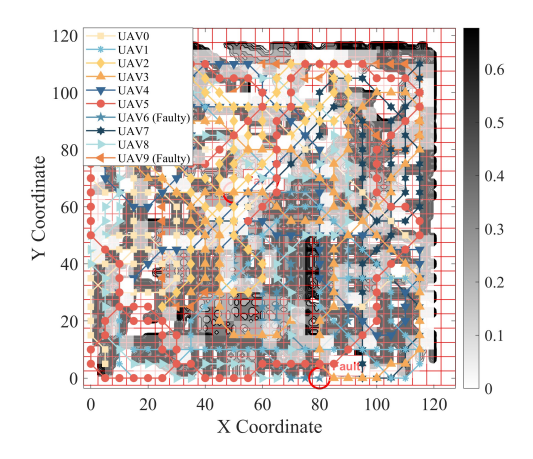


Figure 5. 10 UAVs: High-Probability region paths.

| Time | GS | PSO | DEROA |
|------|-----------------------------|-----------------------------|------------------------------|
| 30 | $0.34 \pm (4.42e-3)$ | $0.63 \pm (4.83\text{e-}3)$ | $0.70 \pm (4.05\text{e-}3)$ |
| 40 | $0.40 \pm (4.68e-3)$ | $0.77 \pm (6.36e-3)$ | $0.82 \pm (2.20 \text{e-3})$ |
| 50 | $0.45 \pm (2.79e-3)$ | $0.85 \pm (2.95\text{e-}3)$ | $0.87 \pm (2.69 \text{e-3})$ |
| 60 | $0.50 \pm (2.83\text{e-}3)$ | $0.89 \pm (2.13\text{e-}3)$ | $0.91 \pm (2.09e-3)$ |
| 70 | $0.53 \pm (6.09\text{e-}3)$ | $0.95 \pm (6.73\text{e-}4)$ | $0.94 \pm (2.37e-3)$ |
| 80 | $0.59 \pm (7.60e-3)$ | $0.95 \pm (7.38e-4)$ | $0.97 \pm (4.48e-4)$ |

Table 1. Detailed grid coverage rate results of robustness experiment.

creases by 93.1%-106.6%, and compared to the PSO algorithm, it increases by 2.3%-10.9%. At this time, the algorithm utilizes the global search characteristic of differential evolution to prioritize covering the core regions with a probability greater than 0.8, avoiding the local optimum trap of the GS algorithm.

In high-recognition-time scenarios (60-80 min), the coverage rate of DEROA reaches 0.91-0.97. Compared to GS, it increases by 65.7%-81.8%, and compared to the PSO algorithm, it increases by 1.0%-1.2%. As time prolongs, the rolling optimization mechanism of DEROA continuously updates the path, while PSO falls into local optimum, resulting in stagnant coverage rate growth. The growth rate decreases from 10.9% at 30 min to 1.0% at 60 min. DEROA demonstrates better capability of continuous expansion coverage.

4.3.3 Planning Quality Experiment Results and Analysis:

In the target discovery probability experiment, under large-scale inspection scenarios, each condition was set with different reconnaissance times, and DEROA, PSO, and GS were run 25 times for each condition. Table 2 lists the total average return and variance of the maximum target discovery probability from 25 path planning results.

| Time | GS | PSO | DEROA |
|------|-----------------------------|-----------------------------|-----------------------------|
| 50 | $0.30 \pm (3.34\text{e-}4)$ | $0.39 \pm (1.43\text{e-}4)$ | $0.40 \pm (1.22e-4)$ |
| 70 | $0.38 \pm (2.51\text{e-4})$ | $0.47 \pm (9.43e-5)$ | $0.48 \pm (1.93\text{e-}4)$ |
| 90 | $0.42 \pm (1.86\text{e-4})$ | $0.53 \pm (1.91\text{e-}5)$ | $0.54 \pm (1.11\text{e-4})$ |
| 110 | $0.46 \pm (2.72e-4)$ | $0.57 \pm (5.87e-5)$ | $0.58 \pm (1.72\text{e-4})$ |
| 130 | $0.50 \pm (1.63\text{e-}4)$ | $0.60 \pm (5.83\text{e-}5)$ | $0.61 \pm (4.87e-5)$ |
| 150 | $0.52 \pm (2.60\text{e-}4)$ | $0.61 \pm (3.15\text{e-}5)$ | $0.62 \pm (2.67\text{e-}5)$ |

Table 2. Detailed maximum target discovery probability results of planning quality experiment.

DEROA's maximum target discovery probability increased from 0.40 (50min) to 0.62 (150min), representing improvements of 19.2%-33.8% over GS and 1.2%-2.9% over PSO.

As reconnaissance time increased, DEROA exhibited significantly superior stability in probability growth compared to the other algorithms. Within the 50-150min range, its hourly probability increase rate was 0.133%, which is 6.4% higher than PSO (0.125%/hour) and 35.7% higher than GS (0.098%/hour), demonstrating its sustained optimization capability in long-duration missions.

Runtime comparison results are presented to analyze the computational efficiency of the algorithms. Table 3 details the average computation time for the three algorithms across different reconnaissance times. DEROA's runtime increased from 4.17 seconds at 50 min to 12.81 seconds at 150 min, exceeding the runtimes of both GS and PSO. This higher computational complexity stems from operations like Bayesian probability map updates, multi-UAV state interactions, and multi-layer information fusion.

| Working time | GS(s) | PSO(s) | DEROA(s) |
|--------------|-------|--------|----------|
| 20 | 0.26 | 0.39 | 0.48 |
| 50 | 0.72 | 0.94 | 1.12 |
| 80 | 1.23 | 1.52 | 2.09 |
| 110 | 1.64 | 2.37 | 2.56 |
| 140 | 2.00 | 3.64 | 4.42 |
| 170 | 3.38 | 3.84 | 4.21 |
| 200 | 4.17 | 4.56 | 5.24 |
| 230 | 5.75 | 7.76 | 9.12 |
| 260 | 6.99 | 9.78 | 10.63 |
| 290 | 7.88 | 10.89 | 12.81 |

Table 3. Runtime results for planning quality experiment.

Considering detection efficacy, DEROA's computational overhead is justified by significant gains in scenarios prioritizing "detection accuracy first." For instance, at 150 min, its 1.2% higher discovery probability over PSO could correspond to discovering substantially more critical targets (e.g., disaster sites, anomalous areas) in real-world applications, far outweighing the impact of the time cost.

From an engineering perspective, DEROA's computation time remains acceptable (e.g., 12.81 seconds for a 150 min mission). Furthermore, runtime efficiency can be further enhanced through hardware upgrades and algorithmic parallelization optimizations.

5. Conclusions and Prospects

5.1 Conclusions

This study addresses the challenges of high uncertainty in target distribution and inefficient inspection path planning for multi-UAV cooperative target perception. By designing a multi-layer information fusion probabilistic quantification map model, a Differential Evolution-based Rolling Optimization Cooperative Algorithm (DEROA), and dynamic reward functions with path optimization strategies, we achieve significant improvements in high-probability area coverage, substantial reductions in flight turns, increased target discovery probability, and robust algorithm performance.

5.2 Future Work

Despite the progress achieved, several areas warrant further investigation. Future research could extend heterogeneous UAV swarm collaboration mechanisms to optimize task allocation strategies for mixed formations of fixed-wing and rotary-wing UAVs. Additionally, advancing cross-domain cooperative systems-particularly the in-depth application of integrated airground sensor network task chains in scenarios such as disaster emergency response-represents a critical direction for exploration

Acknowledgements

This work is jointly supported by National Key Research and Development Program of China under grant (No. 2024YFF1400804) and Program of Song Shan Laboratory (Included in the Management of Major Science and Technology Program of Henan Province) (No. 221100211000-03).

References

- Alexan, W., Aly, L., Korayem, Y., Gabr, M., El-Damak, D., Fathy, A., Mansour, H. A., 2024. Secure communication of military reconnaissance images over UAV-assisted relay networks. *IEEE Access*.
- Asadzadeh, S., de Oliveira, W. J., de Souza Filho, C. R., 2022. UAV-based remote sensing for the petroleum industry and environmental monitoring: State-of-the-art and perspectives. *Journal of Petroleum Science and Engineering*, 208, 109633.
- Baek, H., Lim, J., 2018. Design of future UAV-relay tactical data link for reliable UAV control and situational awareness. *IEEE Communications Magazine*, 56(10), 144–150.
- Boccardo, P., Chiabrando, F., Dutto, F., Giulio Tonolo, F., Lingua, A., 2015. UAV deployment exercise for mapping purposes: Evaluation of emergency response applications. *Sensors*, 15(7), 15717–15737.
- Elamin, A., El-Rabbany, A., 2022. UAV-based multi-sensor data fusion for urban land cover mapping using a deep convolutional neural network. *Remote sensing*, 14(17), 4298.
- Hashesh, A. O., Hashima, S., Zaki, R. M., Fouda, M. M., Hatano, K., Eldien, A. S. T., 2022. AI-enabled UAV communications: Challenges and future directions. *IEEE Access*, 10, 92048–92066.
- Hügler, P., Grebner, T., Knill, C., Waldschmidt, C., 2020. UAV-borne 2-D and 3-D radar-based grid mapping. *IEEE Geoscience and Remote Sensing Letters*, 19, 1–5.
- Li, S., Jia, Y., Yang, F., Qin, Q., Gao, H., Zhou, Y., 2022. Collaborative decision-making method for multi-UAV based on multiagent reinforcement learning. *IEEE Access*, 10, 91385–91396.
- Liang, J., Guo, H., Chen, K., Yu, K., Yue, C., Li, X., 2023. An improved Kalman particle swarm optimization for modeling and optimizing of boiler combustion characteristics. *Robotica*, 41(4), 1087–1097.
- Peng, Q., Wu, H., Li, N., 2022. Modeling and solving the dynamic task allocation problem of heterogeneous UAV swarm in unknown environment. *Complexity*, 2022(1), 9219805.
- Rachman, E., Razali, R., 2011. A mathematical modeling for design and development of control laws for unmanned aerial vehicle (UAV). *International Journal of Applied Science and Technology*, 1(4).

- Shahbazi, M., Sohn, G., Théau, J., Menard, P., 2015. Development and evaluation of a UAV-photogrammetry system for precise 3D environmental modeling. *Sensors*, 15(11), 27493–27524
- Sun, Y., Tong, X., Lei, Y., Guo, C., Lei, Y., Song, H., An, Z., Tang, J., Wu, Y., 2024. A multi-scale path-planning method for large-scale scenes based on a framed scale-elastic grid map. *International Journal of Digital Earth*, 17(1), 2383852.
- Wu, X., Lei, Y., Tong, X., Zhang, Y., Li, H., Qiu, C., Guo, C., Sun, Y., Lai, G., 2022. A non-rigid hierarchical discrete grid structure and its application to UAVs conflict detection and path planning. *IEEE Transactions on Aerospace and Electronic Systems*, 58(6), 5393–5411.
- Xiao, S., Tan, X., Wang, J., 2021. A simulated annealing algorithm and grid map-based UAV coverage path planning method for 3D reconstruction. *Electronics*, 10(7), 853.
- Xu, C., Xu, M., Yin, C., 2020. Optimized multi-UAV cooperative path planning under the complex confrontation environment. *Computer Communications*, 162, 196–203.
- Yu, T., Tang, J., Bai, L., Lao, S., 2017. Collision avoidance for cooperative UAVs with rolling optimization algorithm based on predictive state space. *Applied Sciences*, 7(4), 329.
- Yu, X., Li, C., Zhou, J., 2020. A constrained differential evolution algorithm to solve UAV path planning in disaster scenarios. *Knowledge-Based Systems*, 204, 106209.
- Zhou, Y., Rao, B., Wang, W., 2020. UAV swarm intelligence: Recent advances and future trends. *Ieee Access*, 8, 183856–183878.